

Liquid crystal control of the plasmon resonances at terahertz frequencies in graphene microribbon gratings

V. Yu. Reshetnyak,¹ V. I. Zadorozhnyi,¹ I. P. Pinkevych,¹ and D. R. Evans²

¹*Physics Faculty, Taras Shevchenko National University of Kyiv, Volodymyrs'ka Street 64, Kyiv 01601, Ukraine*

²*Air Force Research Laboratory, Materials and Manufacturing Directorate, Wright-Patterson Air Force Base, Ohio 45433, USA*

(Received 12 March 2017; revised manuscript received 20 June 2017; published 4 August 2017)

We theoretically study the influence of the liquid crystal (LC) orientational state on the absorption, reflection, and transmission spectra of a graphene microribbon grating placed between a nematic LC and an isotropic dielectric substrate. We calculate the absorption, reflection, and transmission coefficients at normal incidence of a far-infrared transverse magnetic wave (THz) and show that control of the orientational state of the LC layer enables the manipulation of the magnitude of the absorption and reflection maxima. The influence the LC orientational state on the plasmonic resonance increases with increasing the isotropic substrate dielectric constant and the graphene microribbon width to grating spacing ratio.

DOI: [10.1103/PhysRevE.96.022703](https://doi.org/10.1103/PhysRevE.96.022703)

I. INTRODUCTION

Surface plasmon-polaritons (SPPs) recently detected in graphene ribbons possess strong mode confinement and lower propagation loss in the midinfrared and far-infrared (THz) spectral region [1–4]. The combination of the relatively high confinement and low losses in graphene ribbons can be regarded as a good alternative for traditional noble metals. Methods used to excite SPPs in graphene have been a diffractive graphene grating etched in a corrugated silicon substrate [5], graphene nanoribbons on different supporting substrates [6], a graphene monolayer on a silicon-based graded grating structure [7], or a graphene layer on a substrate composed of a dielectric spacer and a transparent conductive wafer with a periodic interface relief [8]. There are also other schemes based on using graphene sheets with a periodically modulated conductivity, relief corrugations, etc. (see, for example, Refs. [9,10]). In all of these cases, the need for the presence of gratings is caused by the huge wave vector mismatch between the graphene plasmonic wave and the incident electromagnetic wave [11].

In recent years, various devices utilizing surface plasmon excitation in graphene nano- and microribbon structures, in particular tunable absorbers [4,12,13] and modulators [14], were proposed. By adjusting the permittivity of substrates or the Fermi energy of the ribbon's structures, one can change the IR and THz absorbance, transmittance, and reflectance in graphene based devices. The Fermi energy can be changed by applying a gate voltage [15,16] or by chemical doping in the absence of any bias [17]. One more way to excite and control the SPP propagation in graphene is the use of a uniaxial substrate with the surface parallel to the principal axes [18]. In such a scheme, the momentum of the SPP depends on the propagation direction.

SPPs in active plasmonic devices can be controlled by driving the liquid crystal (LC) in a variety of ways, using, for example, electric fields, light, surface acoustic waves or heat (see Ref. [19] and reference within). In graphene structures the resonant plasmon frequency depends on the dielectric properties of layers placed above and below the graphene sheet or ribbon. The LC dielectric permittivity depends on the LC

director, which can be tuned by reorienting the director using external electric or magnetic fields.

In the present study, we propose to place the LC slab near the graphene microribbon grating and control the absorption, reflection, and transmission of this structure in the terahertz regime by reorienting the LC director.

II. EQUATIONS FOR ELECTRIC AND MAGNETIC VECTORS OF THE TM-WAVE

Consider a graphene microribbon grating in the xy plane placed between a nematic LC layer (anisotropic top substrate) and an isotropic dielectric substrate. Each microribbon in the grating is a single layer graphene with the ribbon along the y axis, where d is the microribbon width and Λ is the grating spacing (Fig. 1).

A plane monochromatic wave propagates along the z axis from the side of the LC and excites the plasmons in the graphene microribbons. We assume semi-infinite substrates that allows us to neglect the effects of multiple reflections; in the y direction the system is infinite.

To simplify calculations, we suppose the LC director to be only reoriented in the xz plane, where the angle ψ describes the director deviation from the z axis. We also set the magnetic vector of the incident wave to be perpendicular to the xz plane [transverse magnetic (TM) wave].

Because of the strong confinement of the SPPs in the ribbons, only the thin layer of the LC substrate near the graphene influences the SPPs. Therefore, we can set the LC director orientation in the whole substrate to be homogeneous and equal to the director orientation of this layer near the graphene. For this hypothesis to be valid it is important to use types of LCs with low anchoring energy so that their orientation near the graphene layer can be changed by applying an external electric field. Standard LCs like 5CB and 8CB [20] are not ideal. For example, to reorient the LC 5CB from the planar to homeotropic state in a cell with graphene substrates and thickness $15\ \mu\text{m}$, an external voltage of 45 V is required [21]. Lower voltages could be used with LCs that have lower anchoring energy.

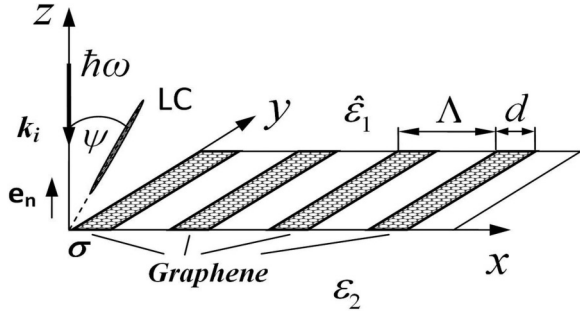


FIG. 1. Schematic of the graphene microribbon grating structure. d is the ribbon width, Λ is the grating spacing, ψ is the director angle with the z axis, $\hat{\epsilon}_1$ is the LC dielectric tensor, ϵ_2 is the isotropic substrate dielectric permittivity, σ is the graphene conductivity, \mathbf{e}_n is a unit normal to the graphene plane in the positive z direction, and \mathbf{k}_i is the wave vector of an incident TM plane monochromatic wave.

The LC optical dielectric tensor can be written in the form $\epsilon_{lij} = n_o^2 \delta_{ij} + (n_e^2 - n_o^2) n_i n_j$, $i, j = x, y, z$, where n_i denotes the components of the director $\mathbf{n} = (\sin \psi, 0, \cos \psi)$; n_o and n_e are the refractive indices of the ordinary and extraordinary waves, respectively [22].

We suppose that the TM wave is normally incident in the LC on the graphene grating. As it follows from the Maxwell equations, electric and magnetic vectors of this wave in the LC take the form

$$\begin{aligned} \mathbf{E}_i &= (E_{ix} \mathbf{e}_x + E_{iz} \mathbf{e}_z) e^{-i(k_iz + \omega t)}, \\ \mathbf{H}_i &= -\frac{k_i}{\omega \mu_0} E_{ix} e^{-i(k_iz + \omega t)} \mathbf{e}_y, \\ E_{iz} &= -(\epsilon_{1xz} / \epsilon_{1zz}) E_{ix}, \end{aligned} \quad (1)$$

with the dispersion equation

$$k_i = \frac{\omega}{c} \sqrt{\epsilon_{1xx} - \frac{\epsilon_{1xz}^2}{\epsilon_{1zz}}}. \quad (2)$$

For reflected and transmitted waves, we use the Fourier-Floquet expansion with respect to the coordinate x . Satisfying the Maxwell equations, the electric and magnetic vectors of these waves can be written as follows:

(i) for the reflected wave,

$$\begin{aligned} \mathbf{E}_r &= \frac{c/(\omega \epsilon_{1zz})}{\sqrt{\epsilon_{1xx} - \frac{\epsilon_{1xz}^2}{\epsilon_{1zz}}}} \sum_n [(\epsilon_{1zz} k_{rn} + \epsilon_{1xz} k_n) \mathbf{e}_x \\ &\quad - (\epsilon_{1xz} k_{rn} + \epsilon_{1xx} k_n) \mathbf{e}_z] a_n e^{i(k_n x + k_{rn} z - \omega t)}, \\ \mathbf{H}_r &= \epsilon_0 c \sqrt{\epsilon_{1xx} - \frac{\epsilon_{1xz}^2}{\epsilon_{1zz}}} \sum_n a_n e^{i(k_n x + k_{rn} z - \omega t)} \mathbf{e}_y, \end{aligned} \quad (3)$$

with the dispersion equation

$$k_{rn} = \sqrt{\left(\epsilon_{1xx} - \frac{\epsilon_{1xz}^2}{\epsilon_{1zz}}\right) \sqrt{\left(\frac{\omega^2}{c^2} - \frac{k_n^2}{\epsilon_{1zz}}\right) - \frac{\epsilon_{1xz}}{\epsilon_{1zz}} k_n}, \quad (4)$$

(ii) for the transmitted wave,

$$\begin{aligned} \mathbf{E}_t &= -\frac{c}{\omega \sqrt{\epsilon_2}} \sum_n (k_{tn} \mathbf{e}_x + k_n \mathbf{e}_z) b_n e^{i(k_n x - k_{tn} z - \omega t)}, \\ \mathbf{H}_t &= \epsilon_0 c \sqrt{\epsilon_2} \sum_n b_n e^{i(k_n x - k_{tn} z - \omega t)} \mathbf{e}_y, \end{aligned} \quad (5)$$

with the dispersion equation

$$k_{tn} = \sqrt{\frac{\omega^2}{c^2} \epsilon_2 - k_n^2}. \quad (6)$$

Here, $k_n = 2\pi n / \Lambda$, where n is the number of a Floquet spatial harmonic.

We define the current density in the plane of the graphene grating as $\mathbf{j}_s = \sigma(x) E_{tx}(z=0) \mathbf{e}_x$, where $\sigma(x) = \sigma$ within each microribbon and $\sigma(x) = 0$ in the gaps between microribbons. Substituting $E_{tx}(z=0)$ from Eq. (5), we obtain

$$\mathbf{j}_s = -\sigma(x) \frac{c}{\omega \sqrt{\epsilon_2}} \sum_n k_{tn} b_n e^{i(k_n x - \omega t)} \mathbf{e}_x. \quad (7)$$

To obtain equations for coefficients a_n, b_n of the Fourier-Floquet expansion Eqs. (3) and (5), we use the boundary conditions

$$\begin{aligned} [\mathbf{e}_n \times (\mathbf{H}_i + \mathbf{H}_r - \mathbf{H}_t) - \mathbf{j}_s]_{|z=0} \mathbf{e}_x &= 0, \\ [\mathbf{e}_n \times (\mathbf{E}_i + \mathbf{E}_r - \mathbf{E}_t)]_{|z=0} \mathbf{e}_y &= 0. \end{aligned} \quad (8)$$

Now we substitute Eqs. (1), (3), and (5) for electric and magnetic vectors and Eq. (7) for the current density \mathbf{j}_s , into Eqs. (8). Then, using the dispersion Eqs. (2), (4), and (6), we arrive at

$$\begin{aligned} \sum_n \left[\sqrt{\epsilon_{1xx} - \frac{\epsilon_{1xz}^2}{\epsilon_{1zz}}} a_n \right. \\ \left. - \left(\sqrt{\epsilon_2} + \sqrt{\frac{\omega^2}{c^2} - \frac{4\pi^2 n^2}{\epsilon_2 \Lambda^2} \frac{\sigma(x)}{\epsilon_0 \omega}} \right) b_n \right] e^{\frac{2i\pi n x}{\Lambda}} \\ - \sqrt{\epsilon_{1xx} - \frac{\epsilon_{1xz}^2}{\epsilon_{1zz}}} E_{ix} = 0, \end{aligned} \quad (9)$$

$$\begin{aligned} \sum_n \left[\sqrt{\frac{\omega^2}{c^2} - \frac{4\pi^2 n^2}{\epsilon_{1zz} \Lambda^2}} a_n + \sqrt{\frac{\omega^2}{c^2} - \frac{4\pi^2 n^2}{\epsilon_2 \Lambda^2}} b_n \right] e^{\frac{2i\pi n x}{\Lambda}} \\ + \frac{\omega}{c} E_{ix} = 0. \end{aligned} \quad (10)$$

Multiplying Eqs. (9) and (10) by $e^{-\frac{2i\pi m x}{\Lambda}}$, where m is an integer and integrating these equations over x in the range $[0, \Lambda]$, we obtain the set of equations for coefficients a_n, b_n :

$$b_n = -\frac{1}{\sqrt{\frac{\omega^2}{c^2} - \frac{4\pi^2 n^2}{\epsilon_2 \Lambda^2}}} \left(\frac{\omega}{c} E_{ix} \delta_{n0} + \sqrt{\frac{\omega^2}{c^2} - \frac{4\pi^2 n^2}{\epsilon_{1zz} \Lambda^2}} a_n \right), \quad (11)$$

$$\begin{aligned}
& \left[\sqrt{\frac{\omega^2}{c^2} - \frac{4\pi^2 n^2}{\varepsilon_{1zz} \Lambda^2}} \left(\frac{\sigma d}{\varepsilon_0 \omega \Lambda} + \frac{\sqrt{\varepsilon_2}}{\sqrt{\frac{\omega^2}{c^2} - \frac{4\pi^2 n^2}{\varepsilon_2 \Lambda^2}}} \right) + \sqrt{\varepsilon_{1xx} - \frac{\varepsilon_{1xz}^2}{\varepsilon_{1zz}}} \right] a_n \\
& + \sum_{m(m \neq n)} \frac{i\sigma \left(e^{\frac{2i\pi(m-n)d}{\Lambda}} - 1 \right) \sqrt{\frac{\omega^2}{c^2} - \frac{4\pi^2 m^2}{\varepsilon_{1zz} \Lambda^2}}}{2\pi\omega\varepsilon_0(n-m)} a_m \\
& = \left[\sqrt{\varepsilon_{1xx} - \frac{\varepsilon_{1xz}^2}{\varepsilon_{1zz}}} - \frac{\sigma d}{\varepsilon_0 c} - \frac{\sqrt{\varepsilon_2} \omega / c}{\sqrt{\frac{\omega^2}{c^2} - \frac{4\pi^2 n^2}{\varepsilon_2 \Lambda^2}}} \right] E_{ix} \delta_{n0} \\
& + \frac{i\sigma(1 - e^{-\frac{2i\pi nd}{\Lambda}})}{2\pi\varepsilon_0 n c} E_{ix} (1 - \delta_{n0}). \quad (12)
\end{aligned}$$

In the infrared and terahertz spectral regions the intraband contribution to the graphene conductivity dominates. Then, in the random phase approximation the two-dimensional conductivity of graphene can be written as [1]

$$\sigma = \frac{e^2 E_F}{\pi \hbar^2} \frac{\tau i}{\omega \tau + i}, \quad (13)$$

where E_F is the Fermi energy of graphene, τ is the electron relaxation time, and e is the electron charge.

The reflection and transmission coefficients are defined as

$$\begin{aligned}
R &= |\text{Re}(\mathbf{E}_r \times \mathbf{H}_r^*)| / |\text{Re}(\mathbf{E}_i \times \mathbf{H}_i^*)|, \\
T &= |\text{Re}(\mathbf{E}_t \times \mathbf{H}_t^*)| / |\text{Re}(\mathbf{E}_i \times \mathbf{H}_i^*)|. \quad (14)
\end{aligned}$$

The graphene absorption coefficient is $A = 1 - (R + T)$. Numerically solving Eqs. (11)–(13) the coefficients a_n , b_n are obtained. Using Eqs. (3) and (5) to find the electric and magnetic vectors of the reflected and transmitted waves and after their substitution into Eq. (14), we calculate the reflection, transmission, and absorption coefficients.

III. RESULTS AND DISCUSSION

As material of the nematic layer, we use the high birefringence ($n_e - n_o \approx 0.41$) LC mixture W1791 with $n_o \approx 1.53$, $n_e \approx 1.94$ at $\lambda = 1.064 \mu\text{m}$ [23]. The birefringence of W1791, which is known in visible and near-IR regions of spectrum, was extrapolated to mid-IR and THz frequencies using the extended Cauchy dispersion formulas obtained for the LC mixture E7 [24]. It is worth mentioning that such extrapolation into transparent but sufficiently remote spectral area can give a substantial error and then the values must be considered as an estimation. In our study, we chose either a low dielectric constant material (e.g., hexagonal boron nitride, h-BN, $\varepsilon_2 = \varepsilon_{h\text{-BN}} = 3$) [25,26] or a high dielectric constant material (silicon, Si, $\varepsilon_2 = \varepsilon_{\text{Si}} = 11.7$) [27] as the isotropic substrate material.

For evaluation of the electron relaxation time we used the formula $\tau = \mu E_F / (e v_F^2)$, where μ is the carrier mobility, $v_F = 3 \times 10^6 \text{ m} \cdot \text{s}^{-1}$ was the Fermi velocity in graphene [11]. Setting $E_F = 0.64 \text{ eV}$ [1,11,28] and the carrier mobility $\mu = 0.5 \text{ m}^2 / (\text{V} \cdot \text{s})$ we get the carrier scattering time $\tau = 0.32 \text{ ps}$. The simulations were performed in the wavelength ranges 15–55 μm (20–5.45 THz) and 9–15 μm (33.3–20 THz) with a temperature $T = 300 \text{ K}$.

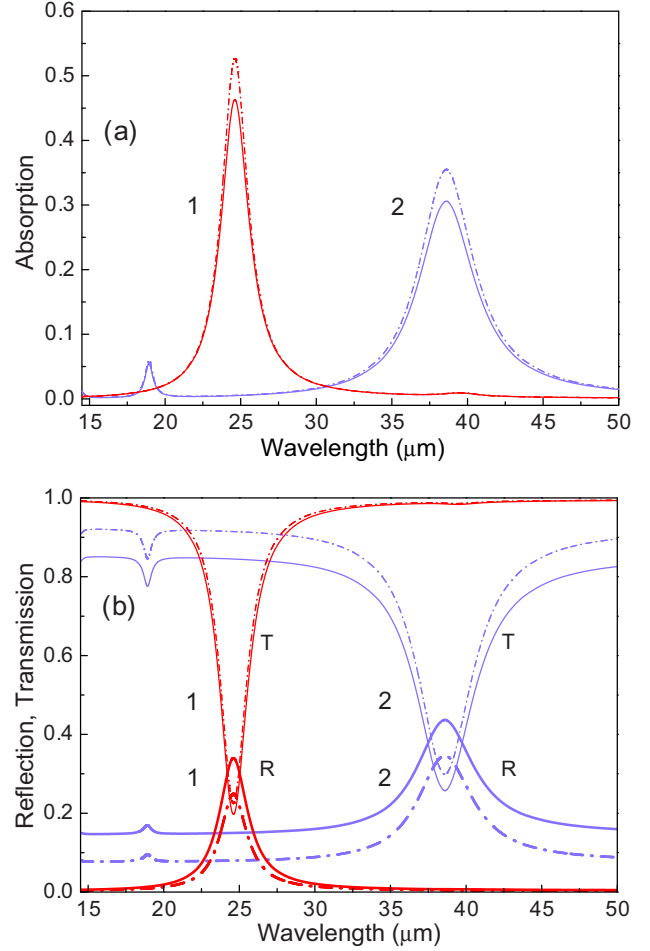


FIG. 2. Absorption (a), reflection, and transmission (b) spectra of the graphene microribbon grating at different angles of the nematic director and for different substrate dielectric permittivity values. $\psi = 0^\circ$, solid line; $\psi = 90^\circ$, dash-dot line. Substrate dielectric constant: $\varepsilon_2 = 3$, curves 1; $\varepsilon_2 = 11.7$, curves 2. Grating spacing, $\Lambda = 1 \mu\text{m}$; ribbon width, $d = 0.5 \mu\text{m}$.

Note that for the parameter values used here for calculations, the Fourier components of the transmitted and reflected fields with $n \neq 0$ are evanescent and do not carry power. However, including these components is necessary to ensure a convergence of the computational procedure. To ensure the required accuracy of calculations, it was necessary to select a number of harmonics $N > 400$ in Eqs. (11) and (12). Results of our numerical calculations of absorption, reflection, and transmission spectra of the graphene grating are shown in Figs. 2–4 for the wavelength range 15–55 μm , and in Fig. 5 for absorption in the wavelength range 9–15 μm .

Figure 2 illustrates the change of the absorption, reflection, and transmission spectra of the graphene grating for two limiting values of the LC director angle $\psi = 0$ and $\psi = 90^\circ$, and a ribbon width to grating spacing ratio $d/\Lambda = 0.5$. Curves 1 and 2 correspond to the cases of an isotropic substrate with either a low or a high dielectric constant, respectively. Maxima in the absorption and reflection spectra are related to the excitation of the plasmons in the graphene microribbons. Within our frequency range, two plasmon peaks in curves 2 are observed. The ratio of the resonant frequencies corresponding to these peaks is equal to 2, which agrees with the results

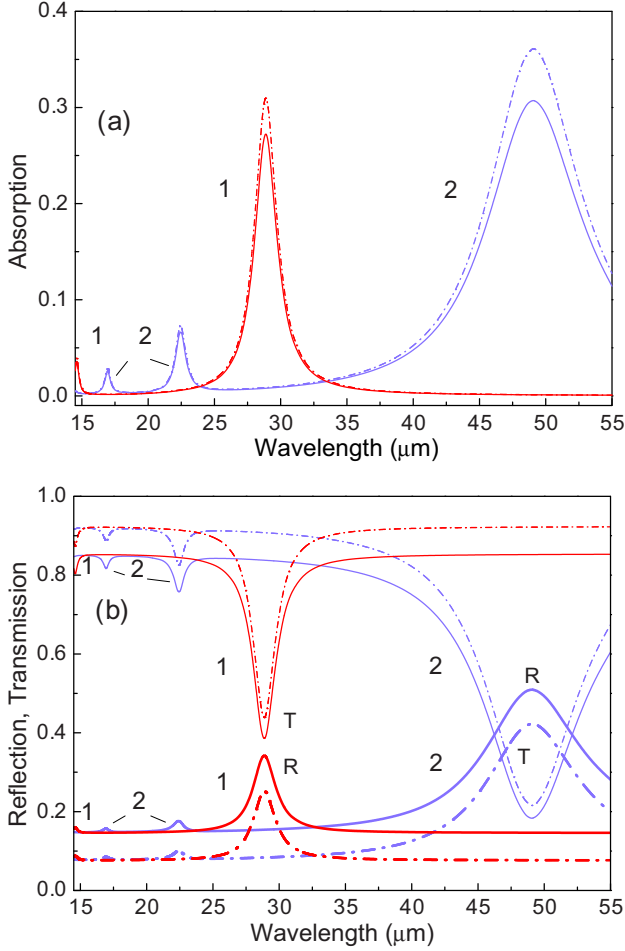


FIG. 3. Absorption (a), reflection, and transmission (b) spectra of the graphene microribbon grating at different angles of the nematic director and for different ribbon aspect ratios at fixed grating spacing. $\psi = 0^\circ$, solid line; $\psi = 90^\circ$, dash-dot line. Ratio $d/\Lambda = 0.3$, curves 1; $d/\Lambda = 0.7$, curves 2. Substrate dielectric constant, $\epsilon_2 = 11.7$; grating spacing, $\Lambda = 1 \mu\text{m}$.

obtained in paper [28] for the graphene grating placed between two isotropic dielectric substrates.

As we can see from Fig. 2, values of these maxima depend on the LC director orientation. In particular, the rotation of the LC director by 90° leads to a change of the absorption maximum value by approximately 14% when $\epsilon_2 = 3$ (h-BN substrate) and by 16% when $\epsilon_2 = 11.7$ (Si substrate).

In Fig. 3, the change of the absorption, reflection, and transmission spectra of the graphene grating at the two limiting values of the LC director angle ψ is shown for two values of the ribbon width to grating spacing ratio, $d/\Lambda = 0.3$ and $d/\Lambda = 0.7$. The grating spacing value is fixed and equal to $\Lambda = 1 \mu\text{m}$. In this case, the rotation of the LC director by 90° leads to the change in the absorption by approximately 14% when $d/\Lambda = 0.3$ and by 18% when $d/\Lambda = 0.7$. A comparison of the results presented in Figs. 2 and 3 shows that the effect of the LC director rotation increases with increasing the isotropic substrate dielectric constant and the ribbon width to grating spacing ratio d/Λ .

In Fig. 4, we compare the absorption, reflection, and transmission spectra at the two values of the director angle

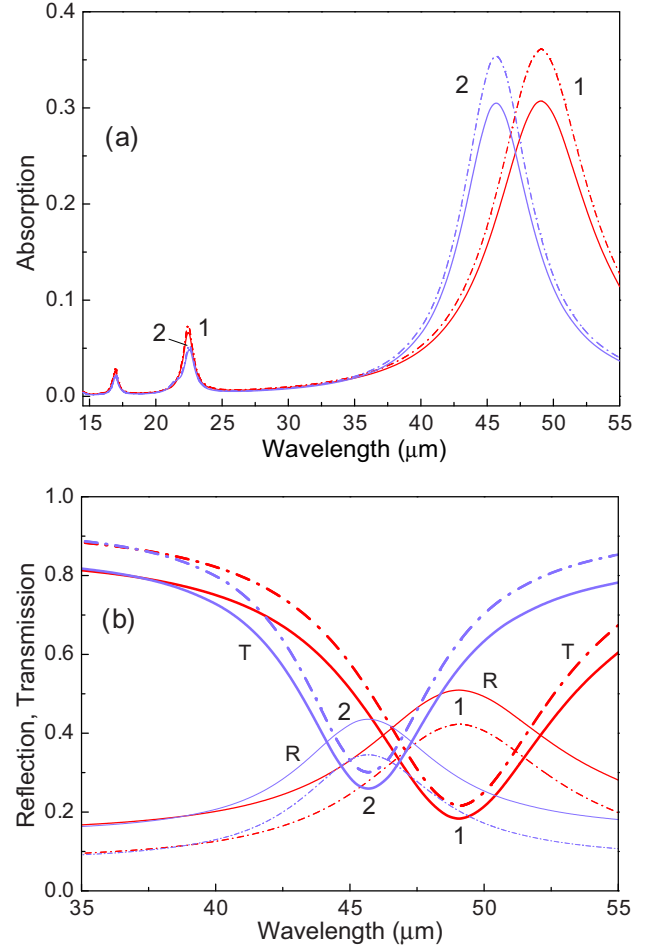


FIG. 4. Absorption (a), reflection, and transmission (b) spectra of the graphene microribbon grating at different angles of the nematic director and for different ribbon aspect ratios at fixed ribbon width. $\psi = 0^\circ$, solid line; $\psi = 90^\circ$, dash-dot line. Ratio $d/\Lambda = 0.7$, curves 1; $d/\Lambda = 0.5$, curves 2. Substrate dielectric constant, $\epsilon_2 = 11.7$; ribbon width, $d = 0.7 \mu\text{m}$.

$\psi = 0$ and $\psi = 90^\circ$ and for the two values of the ribbon width to grating spacing ratio, $d/\Lambda = 0.5$ and $d/\Lambda = 0.7$, holding the ribbon width fixed, $d = 0.7 \mu\text{m}$. In this case, the resonance wavelength shifts due to a change of the grating spacing Λ . However, as in the case of the fixed ribbon width (Fig. 3) the rotation of the LC director by 90° leads to the absorption band maxima increase with increasing the ratio d/Λ , specifically from 16% when $d/\Lambda = 0.5$ to 18% when $d/\Lambda = 0.7$.

The magnitude of the absorption and reflection band maxima decreases with decreasing the ribbon width (see Fig. 2). However, even if the ribbon width decreases significantly, we can compensate it by simultaneous decreasing the grating spacing. For an example, we decreased the ribbon width by approximately one order of magnitude putting $d = 0.05 \mu\text{m}$. Then, holding the ribbon width fixed, the absorption spectra of the graphene grating is calculated for a few values of the grating spacing: $\Lambda = 0.14 \mu\text{m}$ ($d/\Lambda = 0.357$), $\Lambda = 0.1 \mu\text{m}$ ($d/\Lambda = 0.5$), and $\Lambda = 0.078 \mu\text{m}$ ($d/\Lambda = 0.641$).

Results of calculations of the absorption spectra are presented in Fig. 5 for two limiting values of the LC director angle $\psi = 0$ and $\psi = 90^\circ$. As one can see, in this case the plasmon

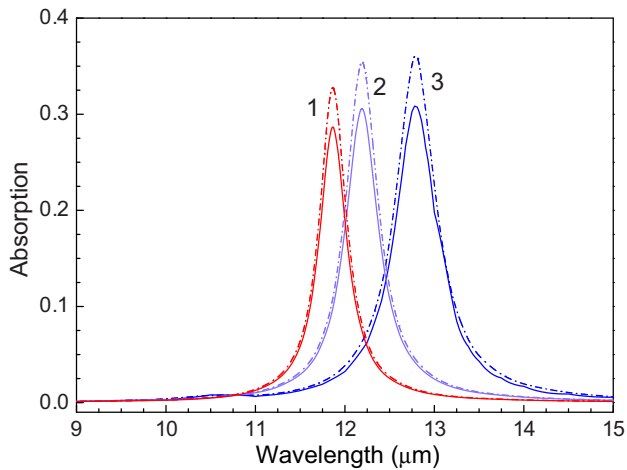


FIG. 5. Absorption spectra of the graphene microribbon grating at different angles of the nematic director and for different ribbon aspect ratios at fixed ribbon width. In this figure, the ribbon width d is 14 times smaller than in Fig. 4. $\psi = 0^\circ$, solid line; $\psi = 90^\circ$, dash-dot line; $d/\Lambda = 0.357$, curves 1; $d/\Lambda = 0.5$, curves 2; $d/\Lambda = 0.641$, curves 3. Substrate dielectric constant, $\epsilon_2 = 11.7$; ribbon width, $d = 0.05 \mu\text{m}$.

resonance wavelengths are shifted into the long-wavelength infrared region (9–15 μm), but the magnitude of the absorption maxima is close to that observed in Figs. 3 and 4. A character of the impact of the LC director rotation on the spectra is also the same: a change in the absorption due to the LC director rotation increases with increasing the ratio d/Λ . Specifically, in this case we obtain an increase of the band maximum from 14.5% for $d/\Lambda = 0.357$ to 17.5% for $d/\Lambda = 0.641$. Reflection and transmission spectra are also similar to those shown in Figs. 3 and 4.

Finally, we note that our results are obtained assuming that the plasmon bands fall into the transparency region of the LC. From Figs. 3–5 we can see that the plasmon resonance wavelength increases with increasing of the graphene ribbon width d and decreasing of the grating spacing Λ . If the LC absorption bands are not very wide it can allow us to shift the plasmon bands into the LC transparency region choosing the corresponding values of the graphene grating spacing or the graphene ribbon width.

IV. CONCLUSIONS

We theoretically studied the influence of the LC orientational state on the SPP absorption, reflection, and transmission spectra of the graphene microribbon grating placed between a nematic LC and an isotropic dielectric. In the far-infrared (20–5.45 THz) and the long-wavelength infrared (33.3–20 THz) regions we observe the maxima in the absorption and reflection spectra which are related to the excitation of the plasmons in the graphene microribbons. We show that the maximum magnitude depends on the LC orientational state. The results suggest that control of the orientational state of the nematic LC layer enables us to manipulate the absorption maximum value within $\sim 18\%$ of its magnitude when using the highly birefringent nematic LC. The influence of the LC director orientation increases with increasing the isotropic substrate dielectric constant and the graphene microribbon width to grating spacing ratio d/Λ . Our results can be used for designing a new type of the graphene microribbon grating structures.

ACKNOWLEDGMENT

This work was partially supported by EOARD Grant No. 15IOE011.

-
- [1] M. Jablan, H. Buljan, and M. Soljačić, *Phys. Rev. B* **80**, 245435 (2009).
 - [2] J. Chen, M. Badioli, P. Alonso-González, S. Thongrattanasiri, F. Huth, J. Osmond, M. Spasenović, A. Centeno, A. Pesquera, P. Godignon, A. Z. Elorza, N. Camara, F. J. García de Abajo, R. Hillenbrand, and F. H. L. Koppens, *Nature* **487**, 77 (2012).
 - [3] Z. Fei, A. S. Rodin, G. O. Andreev, W. Bao, A. S. McLeod, M. Wagner, L. M. Zhang, Z. Zhao, M. Thiemens, G. Dominguez, M. M. Fogler, A. H. Castro Neto, C. N. Lau, F. Keilmann, and D. N. Basov, *Nature* **487**, 82 (2012).
 - [4] L. Ju, B. Geng, J. Horng, C. Girit, M. Martin, Z. Hao, H. A. Bechtel, X. Liang, A. Zettl, Y. R. Shen, and F. Wang, *Nat. Nanotechnol.* **6**, 630 (2011).
 - [5] X.-T. Kong, B. Bai, and Q. Dai, *Opt. Lett.* **40**, 1 (2015).
 - [6] H. Yan, T. Low, W. Zhu, Y. Wu, M. Freitag, X. Li, F. Guinea, P. Avouris, and F. Xia, *Nat. Photonics* **7**, 394 (2013).
 - [7] H. Lu, C. Zeng, Q. Zhang, X. Liu, Md. M. Hossain, P. Reineck, and Min Gu, *Sci. Rep.* **5**, 8443 (2015).
 - [8] Yu. V. Bludov, N. M. R. Peres, and M. I. Vasilevskiy, *Phys. Rev. B* **85**, 245409 (2012).
 - [9] A. Ferreira and N. M. R. Peres, *Phys. Rev. B* **86**, 205401 (2012).
 - [10] T. M. Slipchenko, V. L. Nesterov, L. Martin-Moreno, and A. Yu. Nikitin, *J. Opt.* **15**, 11408 (2013).
 - [11] W. Gao, J. Shu, C. Qiu, and Q. Xu, *ACS Nano* **6**, 7806 (2012).
 - [12] R. Alaei, M. Farhat, C. Rockstuhl, and F. Lederer, *Opt. Express* **20**, 28017 (2012).
 - [13] S. Ke, B. Wang, He Huang, H. Long, K. Wang, and P. Lu, *Opt. Express* **23**, 8888 (2015).
 - [14] C.-C. Lee, S. Suzuki, W. Xie, and T. R. Schibli, *Opt. Express* **20**, 5264 (2012).
 - [15] K. S. Novoselov, A. K. Geim, S. V. Morozov, D. Jiang, Y. Zhang, S. V. Dubonos, I. V. Grigorieva, and A. A. Firsov, *Science* **306**, 666 (2004).
 - [16] J. Kim, H. Son, D. J. Cho, B. Geng, W. Regan, S. Shi, K. Kim, A. Zettl, Y.-R. Shen, and F. Wang, *Nano Lett.* **12**, 5598 (2012).
 - [17] A. Kasry, M. A. Kuroda, G. J. Martyna, G. S. Tulevski, and A. A. Bol, *ACS Nano* **4**, 3839 (2010).
 - [18] I. Arrazola, R. Hillenbrand, and A. Yu. Nikitin, *Appl. Phys. Lett.* **104**, 011111 (2014).

- [19] G. Si, Y. Zhao, E. S. P. Leong, and Y. J. Liu, *Materials*, **7**, 1296 (2014).
- [20] D. W. Kim, Y. H. Kim, H. S. Jeong and H -T. Jung, *Nat. Nanotechnol.* **7**, 29 (2012).
- [21] R. Basu, D. Kinnamon and A. Garvey, *Liq. Crystals* **43**, 2375 (2016).
- [22] P. G. de Gennes and J. Prost, *The Physics of Liquid Crystals*, 2nd ed. (Oxford University Press, Oxford, 1995).
- [23] E. Nowinowski-Kruszelnicki, J. Kędzierski, Z. Raszewski, L. Jaroszewicz, R. Dąbrowski, M. Kojdecki, W. Piecek, P. Perkowski, K. Garbat, M. Olifierczuk, M. Sutkowski, K. Ogrodnik, P. Morawiak, and E. Miszczyk, *Optica Applicata* **42**, 167 (2012).
- [24] J. Li, S. T. Wu, S. Brugioni, R. Meucci, and S. Faetti, *J. Appl. Phys.* **97**, 073501 (2005).
- [25] N. Ohba, K. Miwa, N. Nagasako, and A. Fukumoto, *Phys. Rev. B* **63**, 115207 (2001).
- [26] C. R. Dean, A. F. Young, I. Meric, C. Lee, L. Wang, S. Sorgenfrei, K. Watanabe, T. Taniguchi, P. Kim, K. L. Shepard, and J. Hone, *Nat. Nanotechnol.* **5**, 722 (2010).
- [27] N. K. Emani, Di Wang, T.-F. Chung, L. J. Prokopeva, A. V. Kildishev, V. M. Shalaev, Y. P. Chen, and A. Boltasseva, *Laser Photonics Rev.* **9**, 650 (2015).
- [28] A. Yu. Nikitin, F. Guinea, F. J. Garcia-Vidal, and L. Martin-Moreno, *Phys. Rev. B* **85**, 081405 (2012).